Overcoming Cycle-Skipping Issue using Joint-Domain Full Waveform Inversion

Yu Zhang, Lian Duan, Weishan Han, Feng Chen, Guang Chen and Zhengzheng Zhou, BGP

This paper was prepared for presentation during the 18th International Congress of the Brazilian Geophysical Society held in Rio de Janeiro, Brazil, 16-19 October 2023.

Abstract

The cycle-skipping issue is the main challenge in FWI application. To address this, we propose a Joint-Domain FWI (JDFWI) framework that minimize the travel time misfit in both data and model domains. In the model domain, we use delay time common image gathers (DTCIGs) to measure the travel time inaccuracy. In the data domain, we extract the travel time misfit without relying on the amplitude information. We have applied the proposed JDFWI to several field datasets and found that it successfully overcomes the cycle-skipping issue and improves velocity estimation for complex geologies.

Introduction

Full waveform inversion (FWI) has been an important method to build velocity models for seismic imaging (Tarantola, 1984; Virieux and Operto, 2009). A classical FWI inverts velocity models by iteratively minimizing the difference between the recorded field data and simulated model data. However, two major issues may cause FWI to fail in production: cycle-skipping and amplitude discrepancy between the field and model data, particularly when there are sharp contrasts and large-scale geobodies in the model. When the phases, or traveltime differences, between field and model data are large, the oscillatory pattern of the seismic signals introduces local minima. FWI may attempt to fit the simulated model data to a wrong cycle in the observed field data. Additionally, the amplitude distribution of observed field data is usually very different from that of modeled. If this difference is not appropriately addressed, it will be interpreted as velocity error by FWI, which can lead to the inversion of erroneous velocity models.

Since the traveltime difference of seismic signals is more linearly related to velocity error than waveform difference and any discrepancies in the amplitude difference are inconsequential, extracting the traveltime information of field data effectively lies at the heart of velocity model building and the application of FWI. To achieve this, researchers have made many influential advancements such as adaptive waveform inversion (Warner and Guasch, 2014), dynamic-warping FWI (Ma and Hale, 2013,), time-lag FWI (Luo and Schuster, 1991) and optimal transport FWI (Yang et al., 2018).

All the aforementioned methods are formulated in the conventional data domain only, and their success relies on the extraction of traveltime misfit between recorded field and modeled data. However, extracting traveltime misfit in data domain is not trivial. When geology is complex, the waveforms are complicated, several reflection, refraction or transmission events may overlay each other when they are recorded. On the other hand, if the initial velocity is simple and far away from the correct one, the modeled synthetic waveforms appear much simpler, with significant traveltime and amplitude differences. Therefore, it is not obvious how to correctly measure traveltime misfit by comparing the two datasets. In summary, there is no guarantee that a data domain traveltime misfit based FWI can overcome cycle-skipping issue when the survey geology is complex or when FWI starts from a poor initial velocity model.

In this work, we describe an alternative FWI solution based on the delay time common image gather (DTCIG) to directly measure the travel time inaccuracy in the model domain, which is intuitive in applications and more sensitive to the velocity inaccuracy. Combining our model-domain velocity inaccuracy measure with the conventional data misfit, we derive the formulation of a Joint-Domain FWI (JDFWI) which minimizes the travel time misfit in both data and model domains. Compared to a conventional FWI, applications to both synthetic and field data demonstrate that the proposed JDFWI can retrieve complex velocity models which does not suffer from cycle-skipping, hence is relaxed from the requirements of reliable initial model or low frequency data.

Method

A conventional full-waveform inversion (FWI) is a data driven method which seeks optimal velocity models minimizing the following least-squares misfit objective function between the simulated data $d(\boldsymbol{x_r}; t; \boldsymbol{x_s})$ and the field data $D(\boldsymbol{x_r}; t; \boldsymbol{x_s})$ (recorded at receiver locations $\boldsymbol{x_r}$ due to a specified source location $\boldsymbol{x_s}$):

$$E(v) = \iiint \left(D - d(v)\right)^2 \, dt d\boldsymbol{x_s} d\boldsymbol{x_r}. \qquad (1)$$

Here, in its simplified case of the acoustic, isotropic and constant density wave equation, the simulated data d is predicted using the velocity models $v(\boldsymbol{x})$ by forward propagating wavefield p as follows:

$$\begin{cases} \left(\frac{1}{v(\boldsymbol{x})^2}\frac{\partial^2}{\partial t^2} - \nabla^2\right) p(\boldsymbol{x}; t; \boldsymbol{x_s}) = \delta(\boldsymbol{x} - \boldsymbol{x_s}) S(t), & (2a) \\ d(\boldsymbol{x_r}; t; \boldsymbol{x_s}) = p(\boldsymbol{x_r}; t; \boldsymbol{x_s}), & (2b) \end{cases}$$

where $S(t)$ is the source wavelet and ∇^2 denotes the Laplacian operator.

The nonlinear state-space response, the curse of dimensionality and the imperfect low frequency content in both the model and data often increase the risk for our conventional FWI to be trapped in the local minimum of objective function (1). This is known as the cycle-skipping

issue (Ma and Hale, 2013). As a simple demonstration of the issue, we simulated field data with a 1Hz high passed flat-spectrum wavelet using equations (2a) and (2b). There are 1501 evenly spaced shots with 10m spacing and 301 evenly spaced receivers with 50m spacing across the 15km wide exact 2D velocity model as shown in Figure (1a). A typical common receiver field data for the receiver at 2km in lateral direction is presented in Figure 2a. Starting with an initial model presented in Figure 1b, the conventional FWI using objective function (1) established an inversion result in Figure 1c. While the inverted model (Figure 1c) matches well with the exact model (Figure 1a) in the shallow section down to 3km, the cycle-skipping issue is straightforward to be concluded in the deeper section with an unphysical velocity update in the wrong direction (the combination lack of low frequency below 1Hz and wavelet sidelobe). However, in contrast, only comparing the field data in Figure 2a and the simulated data in Figure 2c (generated using inverted model in Figure 1c), the cycle-skipping can be a great challenge to conclude.

With this observation, to overcome the long-standing cycle-skipping issue, travel time misfit in the model domain could be an important addition to our conventional data driven FWI objective function (1). Following the computational cost and velocity sensitivity reported in Sava and Fomel (2006), we employ delay time common image gathers (DTCIGs) to form our Joint Domain FWI (JDFWI). The algorithm to generate DTCIGs can be summarized as forward propagation of the source wavefield P_s:

$$\begin{cases} \left(\frac{1}{v(\boldsymbol{x})^2}\frac{\partial^2}{\partial t^2} - \nabla^2\right) P_{\mathrm{S}}(\boldsymbol{x};t;\boldsymbol{x}_s) = 0, & (3a) \\ P_{\mathrm{S}}(\boldsymbol{x};t;\boldsymbol{x}_s) = \delta(\boldsymbol{x}-\boldsymbol{x}_s)g(t), & (3b) \end{cases}$$

and backward propagation of the receiver wavefield P_r by reducing time:

$$\begin{cases} \left(\frac{1}{v(\boldsymbol{x})^2}\frac{\partial^2}{\partial t^2} - \nabla^2\right) P_{\mathrm{R}}(\boldsymbol{x};t;\boldsymbol{x}_s) = 0, & (4a) \\ P_{\mathrm{R}}(\boldsymbol{x};t;\boldsymbol{x}_s) = \delta(\boldsymbol{x}-\boldsymbol{x}_r)D(\boldsymbol{x}_r;t;\boldsymbol{x}_s). & (4b) \end{cases}$$

With τ being the delay time, the DTCIG $R(\boldsymbol{x};\tau)$ can be generated using:

$$R(\boldsymbol{x};\tau) = \iiint P_s(\boldsymbol{x};t-\tau;\boldsymbol{x}_s)P_R(\boldsymbol{x};t+\tau;\boldsymbol{x}_s)\,dt\,d\boldsymbol{x}_s. \quad (5)$$

To demonstrate its sensitivity to the velocity, a DTCIG for our exact 2D benchmark velocity model (Figure 1a), the initial model (Figure 1b) and the conventional FWI inverted model (Figure 1c) are presented in Figures 3a, 3b and 3c, respectively. For the correct velocity, the diving waves in the forward and backward propagation meet along the ray path at the correct timing, their energy thus focuses at zero-lag ($\tau = 0$) delay time on the DTCIG as indicated by the red line in Figure 3a. On the other hand, the poor initial model results the diving waves to defocus as well as to be carried away from the correct timing indicated by the zero-lag delay time in red on the DTCIG in Figure 3b. Crucial to our JDFWI, for inaccurate velocity as the one in Figure 1c (with a cycle-skipping issue), the DTCIG can provide an easy quantification and analysis through the focusing of the diving waves and their deviation from the zero-lag delay time. The objective function of the proposed JDFWI is thus as follows (Almomin and Biondi, 2012):

$$E(\tau, v(\tau)) = \iiint \left(D - d(v(\tau))\right)^2 \, d\tau dt d\boldsymbol{x}_s d\boldsymbol{x}_r. \quad (6)$$

Results

In the first example, JDFWI is performed on the 2D benchmark synthetic dataset. The acquisition detail is introduced in the previous section. The exact velocity in Figure 1a has a chalk structure on the left and a large salt body on the right. Both high-velocity structures initiate as shallow as 2km in depth. In the case of FWI, only when these structures are correctly inverted, the model below them can reflect the exact geology. However, in our initial model for FWI (Figure 1b), both high-velocity structures are missing and the difference to the exact velocity can be as large as 2000m/s at many places. As a result, even starting the conventional FWI on seismic data with only 0-1Hz lacking, the inverted model in Figure 1c is cycle-skipped and not retrieving the correct deep structures below 3km. As shown in the Figure 1d, with the aid of the DTCIG, the proposed JDFWI can establish a high-resolution inverted velocity model similar to the exact model in Figure 1a. For rigorous analysis of our method in both data and model domain, we present the simulated data and the DTCIGs using different models in Figure 2 and Figure 3, respectively. Comparing to the seismic data in Figure 2a, the simulated data (Figure 2d) using the JDFWI inverted model (Figure 1d) can closely predicted the far offset diving reflection caused by the salt body as well as the reflection event from the chalk section at the near offsets. Comparing to the DTCIG using the inverted model from the conventional FWI in Figure 3c, the DTCIG using the JDFWI inverted velocity (Figure 3d) has the diving wave energy focused at the zero-lag delay time at all the penetrated depths. This confirms the quality of the proposed JDFWI inversion statistically.

Our final example is a full-azimuth ocean-bottom node (OBN) data from Gulf of Mexico where the water depth is between 1700m to 2900m. An enormous and complicated salt structure is presented in the area under investigation (Figure 4a). The Tilted Transverse Isotropy (TTI) models from a salt model building process were used as the initial models to start the proposed JDFWI. The JDFWI was performed on raw hydrophone data. We preformed JDFWI to the joint data and model domains convergence in two frequency bands with a maximum frequency of 10Hz first and then 15Hz. Total 15 iterations in both bands were carried out.

As shown in Figure 4, in the sediment section on the left, the initial velocity model in Figure 4a suggests a velocity profile closely matches the geological information presented in the stacked RTM image (Figure 4c). In the inverted model using JDFWI (Figure 4b), further velocity features are retrieved both inside and outside of the salt bodies and match the structures in the stacked RTM image in great detail (Figure 4d). With the reference of two dashed lines highlighting the geological thread, the reflectivity structure at the sediment section better follows the geology without the unphysical bumps in Figure 4c. As the geology unfolds to the middle basin and the salt, the structure using the JDFWI inverted model has a clearer transition and sharper termination. Especially, as shown in the rectangles, the fault structure, the sediment continuity, and the illumination are all improved in the stacked reflectivity image in Figure 4d over the one using initial velocity in Figure 4c. Furthermore, as highlighted in the

ovals, while the structure is broken using the initial velocity (Figure 4c), the connected structure can be confirmed using the JDFWI inverted velocity (Figure 4d).

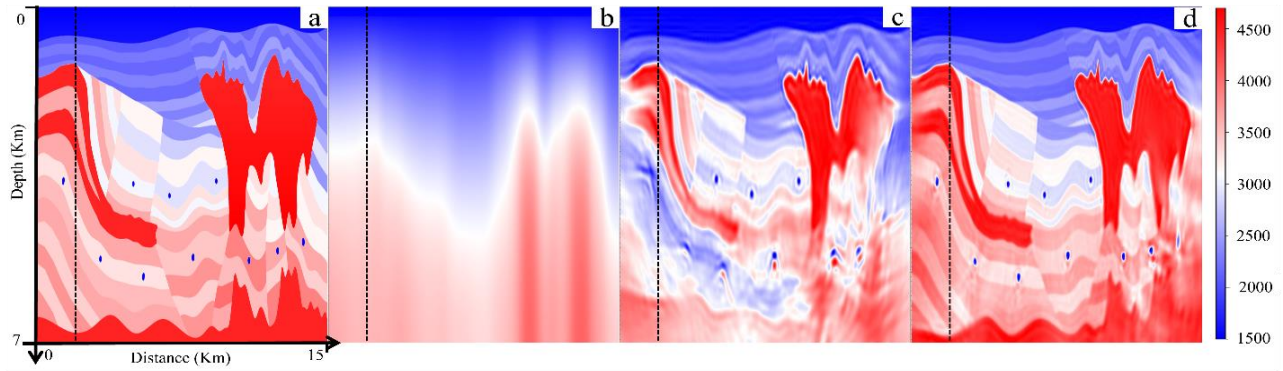

Figure 1 *BGP 2D synthetic example: (a) exact model; (b) initial model; (c) inverted model using conventional FWI with objective function (1); (d) inverted model using JDFWI. Black lines indicate the position of common receiver and DTCIG at 2km lateral direction in Figures 2 and 3.*

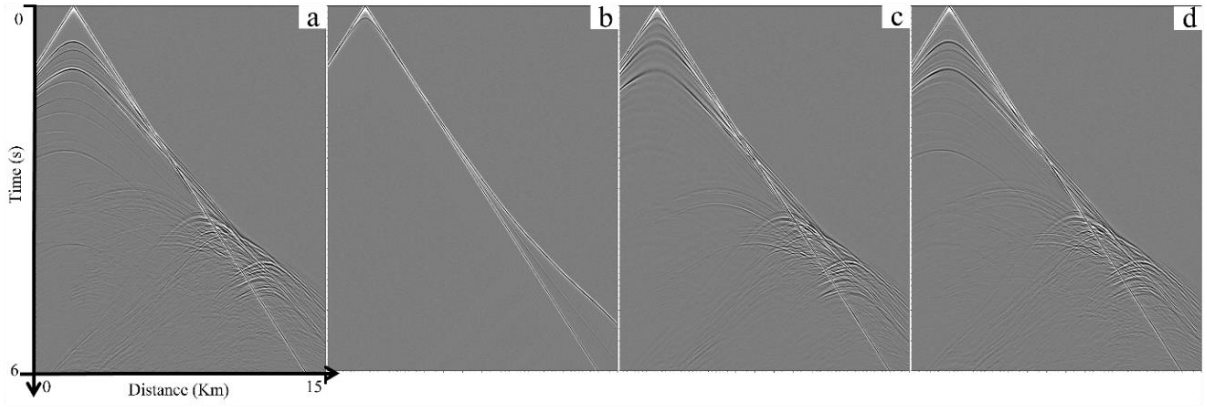

Figure 2 *BGP 2D synthetic example: (a) field data generated using the exact model in Figure (1a); (b) simulated data using the initial model in Figure (1b); (c) simulated data using the inverted model by conventional FWI in Figure (1c); (d) simulated data using the inverted model by JDFWI in Figure (1d).*

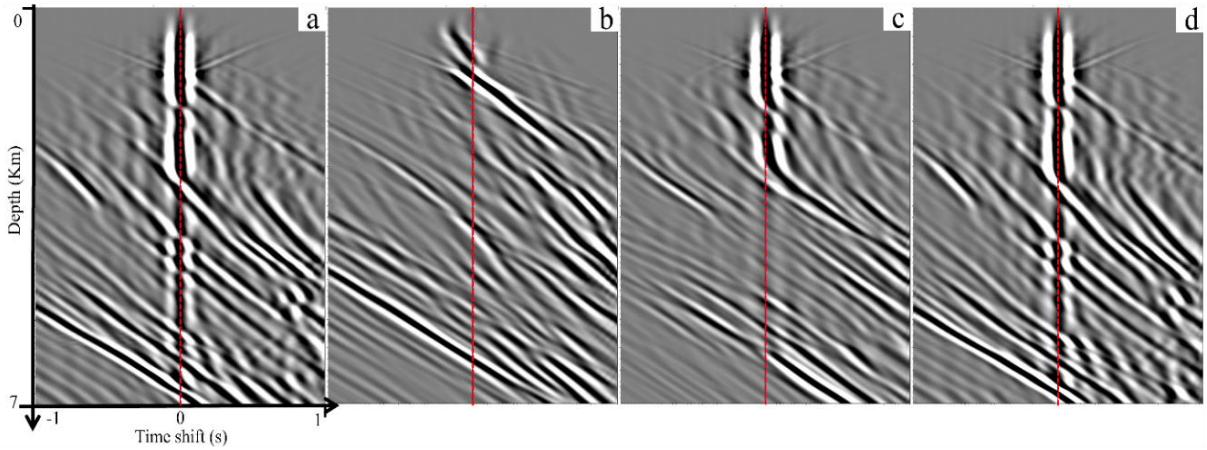

Figure 3 BGP 2D synthetic example: (a) DTCIG generated using the exact model in Figure (1a); (b) DTCIG generated using the initial model in Figure (1b); (c) DTCIG generated using the inverted model by conventional FWI in Figure (1c); (d) DTCIG generated using the inverted model by JDFWI in Figure (1d). Red lines indicate the zero-lag (τ=0) delay time.

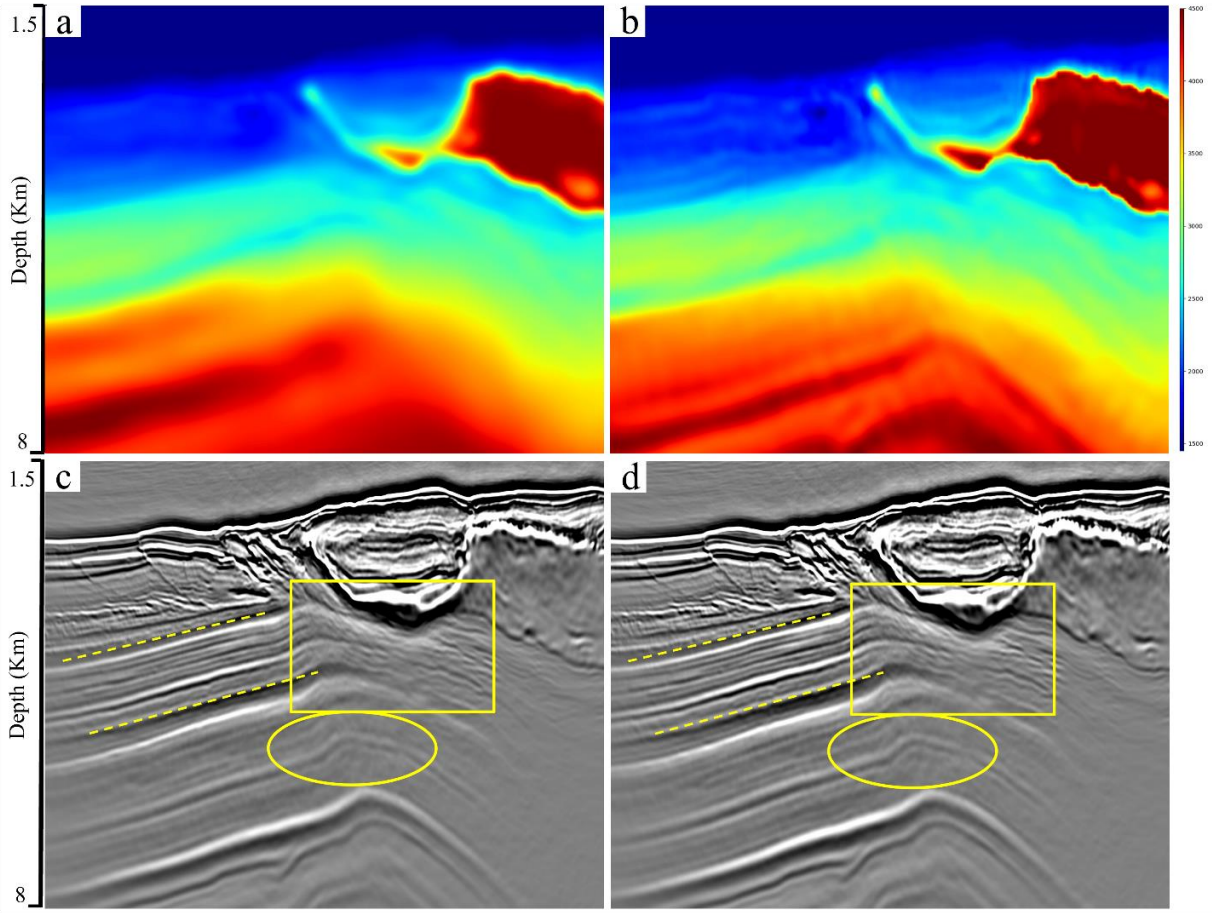

Figure 4 *Gulf of Mexico OBN field example: (a) initial model; (b) inverted model using JDFWI; (c) stacked RTM reflectivity image using the initial model in (a); (d) stacked RTM reflectivity image using the inverted model in (b). The dashed lines indicate the geological thread reference. The rectangles indicate the middle basin structure with sediment termination and subsalt faults. The ovals highlight the deep subsalt turning point of the continuing structure going from the sediment to the subsalt.*

Conclusions

Joint Domain Full Waveform Inversion (JDFWI) provides a practical and efficient framework to invert the seismic data that is immune to cycle-skipping problems. This is achieved by involving the delay time analysis from the delay time common image gathers (DTCIGs) in the data-domain FWI objective function. Application of the proposed JDFWI on the 2D example with complex salt bodies demonstrates that it can overcome the cycle skipping problem due to both poor initial model and lack of low frequency. The results of the Gulf of Mexico ocean-bottom node (OBN) application show improved salt boundary estimation without introducing halo and better subsalt structural continuity and illumination.

Acknowledgments

We thank Shell for the permission to present the data and publish this work. We thank our colleagues for their support, especially Junyong Chang, Guang Chen, Hui Chen, Han Yin and Tiankui Yin.

References

ALMOMIN, A., BIONDI, B. 2012, Tomographic full waveform inversion: practical and computationally feasible approach: 82nd Annual International Meeting, SEG, Expanded Abstracts, 1-5.

LUO, Y., SCHUSTER, G. T. 2012, Wave-equation traveltime inversion: *Geophysics*, **56**, 645-653.

MA, Y., HALE, D. 2013, Wave-equation reflection traveltime inversion with dynamic warping and full-waveform inversion: *Geophysics*, **78**, 223-233.

SAVA, P., FOMEL, S. 2006, Time-shift imaging condition in seismic migration: *Geophysics*, **71**, 209-217.

TARATOLA, A. 1984, Inversion of Seismic Reflection Data in the Acoustic Approximation: Geophysics, **49**,1259-1266

VIRIEUX, J.; OPERTO, S. 2009, An Overview of Full Waveform Inversion in Exploration Geophysics: Geophysics, **74**(6), WCC127-WCC152

WARNER, M., GUASCH, L. 2016, Adaptive waveform inversion: Theory: *Geophysics*, **81**, 429-445.

YANG, Y., ENGQUIST, B., SUN, J. and HAMFELDT, F. 2018, Application of optimal transport and the quadratic Wasserstein metric to full-waveform inversion: *Geophysics*, **83**, 43-62.